Arabian Journal for Science and Engineering (2023) 48:169–179
https://doi.org/10.1007/s13369-022-06899-y

RESEARCH ARTICLE-CHEMISTRY

Synthesized of Zeolite@Ag_2O Nanocomposite as Superb Stability Photocatalysis Toward Hazardous Rhodamine B Dye from Water

Redouane Haounati[1] · Fadi Alakhras[2] · Hassan Ouachtak[3,4] · Tawfik A. Saleh[5] · Ghassab Al-Mazaideh[6] · Eman Alhajri[7] · Amane Jada[8] · Naima Hafid[9] · Abdelaziz Ait Addi[1]

Received: 15 January 2022 / Accepted: 14 April 2022 / Published online: 10 May 2022

Abstract

Over the past years, Ag_2O as an emerging photocatalyst has attracted extensive attention toward the removal of hazardous dye from aqueous media under visible light. However, Ag_2O suffers from major drawbacks such as low stability under sunlight irradiation and high recombination rate of photogenerated electron–hole pairs. In this study, to resolve this problem, a novel nanocomposite-based zeolite clay was successfully prepared using an eco-friendly and economical approach. The nanocomposite Zeolite@Ag_2O (Zeo@Ag_2O) was characterized by X-ray diffraction, scanning electron microscopy, energy dispersive X-ray analysis Fourier transform infrared spectroscopy, Brunauer, Emmett, and Teller surface area method and UV–Vis diffuse reflectance spectroscopy. The obtained nanocomposite exhibited high photocatalytic efficiency for the removal of hazardous Rhodamine B dye from aqueous solution under visible light and the removal rate reached about 100%. Thus, the enhanced photocatalytic activity could be due to the better adsorption ability onto Zeo@Ag_2O nanocomposite surface and the high effective separation of photogenerated electron–hole pairs. Also, the obtained results show that both holes (h +) and hydroxyl radicals (HO°) play an important role in RhB degradation over the synthesized nanocomposite.

Keywords Zeo@Ag_2O nanocomposite · Visible light · Photodegradation · Toxic dyes · Water treatment · Natural zeolite

1 Introduction

During the last few decades, there has been an increase in the pollution load in all the countries. Activities like industrialization and increased urbanization have amplified toxic heavy metals and synthetic dyes pollution in the ecosystem [1], which have numerous awful disasters, from both financial and ecological perspectives [2]. A lot of industrial manufacturing including food, cosmetics, rubber, textiles, paper, plastic, and soft tissues exploit certain materials during the treatment of unprocessed stuff. These materials are called dyes which are organic colored compounds that brought color to different substrates [3]. The dyes that are used in textile processing are divided into different types like basic dyes, reactive dyes, acidic dyes, azo dyes, direct dyes, and disperse dyes[4–6]. The dyes in general have an aromatic structure which makes them stable and non-biodegradable in nature[7]. According to that, dyes are well known in toxicity, carcinogenic, and mutagenic properties. They have severe

✉ Fadi Alakhras
fadialakhras@gmail.com

1 Team of Physical Chemistry and Environment Team, Faculty of Science, Ibn Zohr University, Agadir, Morocco

2 College of Pharmacy, Middle East University, Amman 11831, Jordan

3 Faculty of Applied Science, Ait Melloul, Ibn Zohr University, Agadir, Morocco

4 Applied Chemistry and Environment Laboratory, Applied Bio-Organic Chemistry Team, Faculty of Science, Ibn Zohr University, Agadir, Morocco

5 Department of Chemistry, King Fahd University of Petroleum and Minerals, Dhahran, Saudi Arabia

6 Department of Pharmaceutical Chemistry, College of Pharmacy, University of Hafr Al-Batin, Hafr Al-Batin, Saudi Arabia

7 Department of Chemistry, College of Science, Imam Abdulrahman Bin Faisal University, Dammam, Saudi Arabia

8 Mulhouse Institute of Materials Sciences (IS2M-CNRS), University of Haute Alsace (UHA), 68100 Mulhouse, France

9 Regional Center of Education and Training, Souss-Massa, Morocco

damage to the liver, brain, kidneys, fertility, and nerve system [8]. Moreover, colored water resulting from dyes can harm the marine environment since sunlight could not go through the colored water and impacts the photosynthetic process[9]. It is very essential to control the concentration of colored dyes in waste effluents because of their wide applications and various hazard and toxic properties. Hence, the cleaning of aquatic systems from colored dyes becomes environmentally significant.

Different remediation approaches have been performed for the removal of dyes namely, precipitation, filtration, ion exchange, oxidation, coagulation, ozonation, and adsorption [10–13]. However, the aforementioned methods may have major limitations and drawbacks on the remediation consisting of costly operating process, ineffective at low adsorbate concentration, poor selectivity, and releasing by-toxic species into the environment [14].

In the last few years, the scientific community has shown great interest toward nanomaterials because of their attractive features and numerous technological applications [15]. These nano-structured materials with distinctive properties guide to enhanced qualities for instance: catalysts, adjusted photo-activity, improved strength, and several remarkable features. Nanotechnology is also addressed toward finding solutions to the presented environmental problems. In our time, the photocatalytic process is suggested as one of the most promising approaches for the removal of different toxic and dangerous poisons in addition to environmental remediation [16]. Currently, metal oxide semiconductors have revealed huge research as photocatalysts with great approaching in environmental decontamination and solar energy conversion[17]. Several metal oxides for example: TiO_2, Ag_2O, ZnO, MoO_3, SnO_2, ZrO2, WO_3, $SrTiO_3$, and Fe_2O_3 have been explored as photocatalysts with intensive research [18]. These semi-conductive nanomaterials are active in UV–Vis spectra, nontoxic, biologically inactive, chemically stable, water insoluble, and most importantly cost-effective. When the metal oxide photocatalysts are illuminated with radiation where its energy is equal to or greater than the band gap energy of the photocatalyst, the photons are absorbed yielding photo-generated charge carriers. These charge carriers are very reactive and responsible for the creation of destructive species (OH − ions and superoxide radicals) which are sufficiently strong to oxidize and decompose or decolorize toxic organic pollutants [19–22].

Silver oxide (Ag_2O) is eminent semiconductive material that has enormous applications due to its electrochemical, electronic, optical, and anti-bacterial properties [23, 24]. It is largely exploited in oxidation catalysis, fuel cells, sensors, solar cells, optical switching tools, and biological probes[25]. Silver oxide nanoparticles have band gap energy of 1.2 eV which gives very strong decolorizing capacity utilized in the photocatalytic decomposition of organic dyes in water systems [17, 25–27]. Recently, silver-containing nanoparticles like Ag_2O, Ag_3VO_4, Ag_3PO_4, and Ag_2CO_3 demonstrate tremendous photocatalytic properties in the purpose of pollutants removal which is quite better than other visible light photocatalysts such as N-TiO_2, Zn_2S, and $BiVO_3$ [28]. Accordingly, Ag_2O nanoparticles are considered as one of the most desirable photocatalysts.

However, the major problem associated with the utilizing of metal oxide nanoparticles in wastewater treatment is to promote the post-separation process and slow down the rapid aggregation that noticeably reduces the surface area which has a negative impact on the photocatalytic efficiency [29] 30. The drawbacks can practically be solved by applying certain supports such as clay, glass, activated carbon, and synthetic or natural zeolite [31, 32]. Comparative photocatalytic study was investigated in aqueous solution under UV-light where two nanocomposites (TiO_2-Zeolite and ZnO-Zeolite) were successfully investigated for the removal of Rhodamine B dye [29]. The employment of natural zeolites as adsorbent material has concerned significant interest because of their structural and chemical features. Natural zeolites are abundant, non-toxic, cheap, chemically and thermally stable and consequently are excellent materials for water remediation [33–35].

This study is a continuance of our preceding work where natural zeolite was used as a supporting material of TiO_2 and ZnO nanoparticles for the photodegradation of cationic dye[29]. In the current study, the natural zeolite is customized with silver in order to synthesize nanocomposite including silver nanoparticles. The zeolite-based photocatalyst is characterized whereas the adsorption equilibrium and kinetic studies are well discussed, and a detailed analysis of the effect of Ag_2O nanoparticles on Rhodamine B removal as a dye model (Rhodamine B dye is a typical triphenyl methane chemical dye that has been widely used and commonly detected in various wastewater) with proper mechanism is accomplished. The outcome of this study will support and assess in finding new types of nanocomposites that will be utilized in wastewater processing which is recognized as an imperative factor for all aspects of life.

2 Materials and Methods

2.1 Reagents

All chemical materials used in this study are purchased from Sigma-Aldrich and used as received. Silver nitrate ($AgNO_3$, MM 169.87 g mol^{-1}, Density 4.35 g cm^{-3}, purity 99.9%), ethanol (CH_3CH_2OH, MM 46.07 g mol^{-1}, 98%), and ammonium hydroxide (NH_3OH, MM 35.04 g/mol, 28%). The zeolite samples [29] are washed several times with deionized

water in order to remove impurities. Then the dried material is crushed and sieved for subsequent experiments.

2.2 Characterization

The natural zeolite sample and Zeo@Ag_2O composite are characterized using different characterization methods. Brunauer–Emmett–Teller (BET) method is performed on Quantachrome surface area analyzer to estimate the surface area and type of porosity. The main functional groups in the range of 4000–400 cm^{-1} are assigned by Fourier-transform infrared spectroscopy using IRAFFINTT-2 spectrometer. The crystal patterns of zeolite and the nanocomposite are recorded by X-ray diffractometer-7000, Shimadzu from 5° to 80° 2θ at a scan rate of 2°/min. The surface morphology analyzed by scanning electron microscopy (SEM) of both tuff and Zeo@Ag_2O nanomaterials is measured on INSPECT S50 microscope. Thermal data (TGA/TDA) of samples are obtained by using Shimadzu Instruments DTG-60 between 24 and 900 °C (in air, 10 °C. min^{-1}). The optical absorption properties are recorded using UV–Vis spectrophotometer JascoV730.

2.3 Preparation of Ag-Zeolite Nanocomposite

Ag-zeolite nanocomposite is prepared as per the following procedure. Around 5.0 g of the natural zeolite is introduced in a flask with 100 mL deionized water. The zeolite tuff is dispersed under the sonication for 2 h whereas the system is purged with nitrogen gas for 30 min. Then, 10 mL of 0.2 M silver nitrate solution is added drop by drop under vigorous stirring, and in dark light-free closed system. After 1 h of stirring, a solution containing 2% ammonia is injected slowly into the mixture. 2 h later, the system is then allowed to reflux for 3 h at 90 °C. Then, the mixture is allowed to cool and is separated by centrifuge. The obtained solid Ag-modified zeolite material (Zeo@Ag_2O) is dried and stored for further experiments.

2.4 Photocatalytic Degradation Experiments of Synthesized Zeo@Ag_2O Nanocomposite

The photocatalytic activity of the as-prepared Zeo@Ag_2O nanocomposite was investigated by decomposition of hazardous RhB dye under sunlight. In typical experiment, 100 mg of Zeo@Ag2O nanocomposite was weighed and mixed with 100 mL of 5 mg L^{-1} RhB aqueous solution at initial pH value of 6. Before sunlight irradiation, the aqueous suspension (RhB dye / Zeo@Ag2O) was magnetically stirred in the dark for one hour to establish adsorption/ desorption equilibrium between the photocatalyst and RhB dye. Next, the magnetic stirring of the mixed suspension was continued and exposed to sunlight irradiation to start the degradation process. At a given time interval (Every 10 min), 2 mL of the suspension was collected from the photocatalytic system, and then the residual RhB concentration was determined using UV–Vis spectrophotometer (Shimadzu UV–Vis spectrometer) with respect to the maximum absorbance at 554 nm. Finally, the degradation efficiency was calculated using the following equation:

$$\text{Degradation efficiency} = \left(\frac{c_0 - c_t}{c_t}\right) \quad (1)$$

where C_t (mg/L) is the concentration of each time period and C_0 (mg/L) is the initial concentration of RhB dye.

3 Results and Discussion

3.1 Characterization

FTIR is usually used to find out information about the main functional groups of the investigated materials. The spectrum of zeolite tuff (Fig. 1a) is supported the typical IR spectrum of natural zeolites where strong peaks are present in the typical range. The O–H stretching vibrations obtained as a result of the intermolecular hydrogen bonding appeared at 3400 cm^{-1}. The symmetric and asymmetric stretching vibrations of O–Si–O and O–Al–O are assigned in the range of 810–800 cm^{-1} and 1025–1100 cm^{-1}[36]. The band at 1650 cm^{-1} represents the bending vibration of H_2O molecules present in the zeolite channels [35]. The Ag_2O modified zeolite material (Fig. 1b) is confirmed by stretching vibration of Ag–O bond that can be observed in the range of 400–800 cm^{-1} [25]. After loading of Ag_2O NPs, it is clear that the intensity of peaks is significantly decreased, showing that Ag_2O NPs are precipitated on the crystal structure

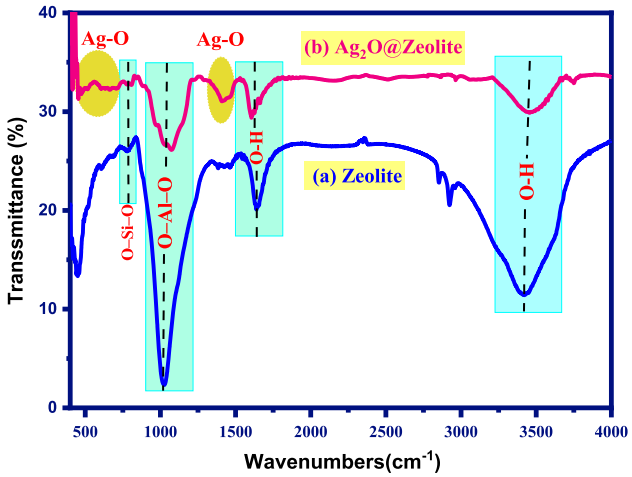

Fig. 1 FTIR spectra of **a** Zeolite, **b** Zeo@Ag_2O nanocomposite

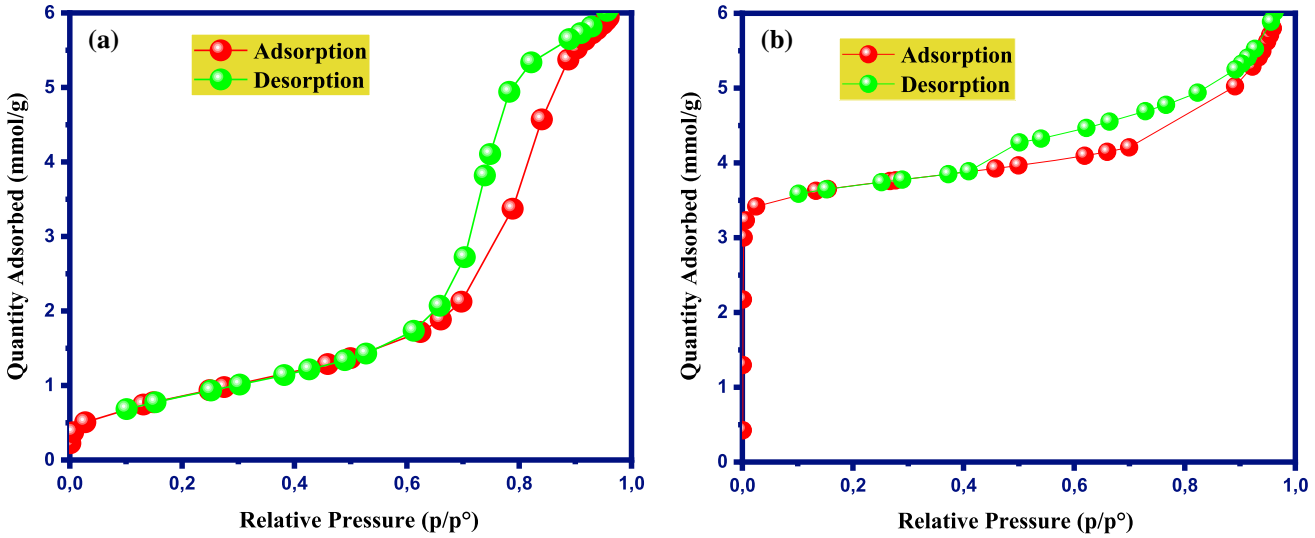

Fig. 2 BET isotherm of **a** Zeolite, **b** Zeo@Ag_2O nanocomposite

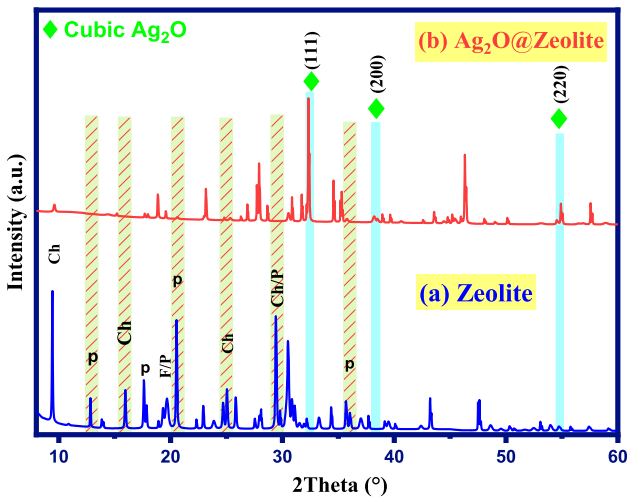

Fig. 3 Powder XRD patterns of **a** zeolite tuff, **b** Zeo@Ag_2O nanocomposite

and then in the porous system of zeolite. These results are in accord with the previously reported studies[37].

The specific surface area and pore size of natural and Ag-modified zeolite samples are determined using the N_2 adsorption–desorption isotherms as depicted in Fig. 2. The BET surface area of zeolite tuff is found to be 69 $m^2\ g^{-1}$ whereas Ag_2O-modified zeolite has a higher surface area reached to 286 $m^2\ g^{-1}$. The positive enhancement in the surface area of the nanocomposite is ascribed to the impregnation of small metal particles on the zeolite which provides extra areas. From Fig. 2 and according to IUPAC classification, the samples fall into the mesoporous category and revealed type IV isotherm [38]. This pattern shows a hysteresis loop which is accompanied with capillary condensation and evaporation in mesoporous materials. The average pore size of unmodified and Ag_2O-impregnated zeolite is 2.6 and 3.1 nm respectively, which is between 2 nm < d < 50 nm [39].

XRD is a common technique of characterization and evaluation of the zeolite framework, where it is used to determine the symmetry and unit cell parameters. The crystalline phases present in zeolite tuff and Ag-zeolite are analyzed and presented in Fig. 3. The pattern of natural zeolite shows intense peaks at 2ϴ of 9.56, 12.93, 20.63, 24.93, 30.65, and 34.32 which corresponds to the zeolite minerals (Ch-chabazite, P-phillipsite, and F-Faujasite) [29].

Moreover, the Ag_2O-modified zeolite nanocomposite depicts new weak to moderate intensity peaks as appeared in Fig. 3b. The new peaks are clearly pointed out the existence of silver nanoparticles decorated the zeolite material and are indexed as a set of lattice planes (111) (200) and (220) (JCPDS, No. 04–0783). All the mineralogy peaks are noticeable and quite strong, which verify the good crystallinity of the studied samples [40]. The crystalline pattern reveals face-centered-cubic (FCC) structure of AgNPs[41].

The surface morphologies of zeolite tuff and Zeo@Ag_2O nanocomposite are investigated by scanning electron microscopy. The SEM image of natural unmodified zeolite displayed in Fig. 4a demonstrates roughness morphology with huge number of cracks and cavities, whereas Fig. 4b shows the SEM analysis of Ag-impregnated zeolite nanoparticles with relatively distinguishable sizes. AgNPs form irregular blocky structures with different shapes. From EDX spectra, it is clearly indicated that silver nanoparticles decorated the zeolite material are presented with relatively high weight percentage.

The thermogravimetric analysis (TGA) and differential thermal analysis (DTA) were used in order to verify the rate of decomposition of water and conversion of Ag_2O into Ag

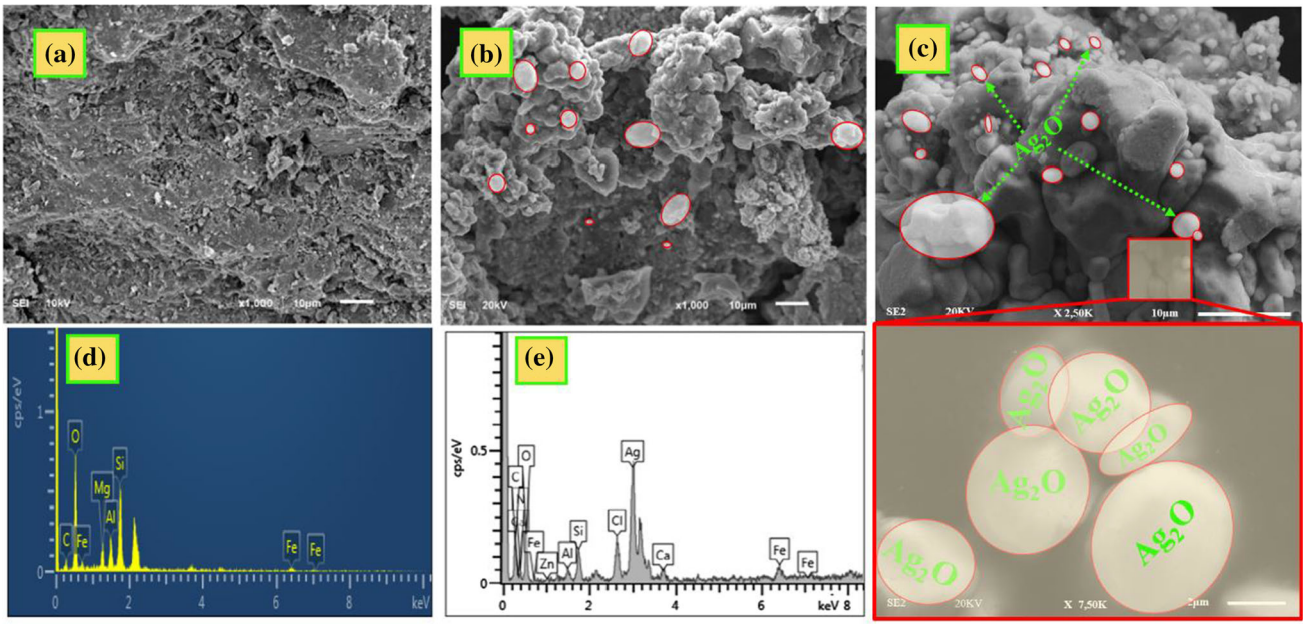

Fig. 4 SEM images and EDX spectrum of **a** and **d** zeolite tuff, **b**, **c**, and **e** Zeo@Ag_2O nanocomposite

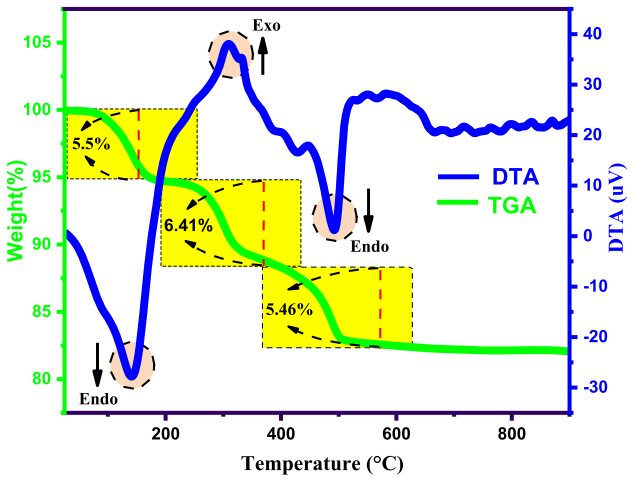

Fig. 5 The TGA and DTA curve of Zeo@Ag_2O nanocomposite

nanoparticles in the zeolite surface and then studied the stability of as-prepared nanocomposite. Figure 5 shows TGA and DTA curves of Zeo@Ag_2O nanocomposite in air from 25 °C to 900 °C. In which the weight loss observed between 100 °C and 190 °C is continuous, the total loss in this range reached about 5.5% which is mainly due to an endothermic reaction at 145 °C for removal of physically adsorbed water. The second total weight loss with about 6.41% occurred from 250 °C to 370 °C with an exothermic reaction at 305 °C, which is most likely attributed to the decomposition of Ag_2O compounds to Ag and O_2 ($Ag_2O \rightarrow Ag + O_2$) [42]. On the other hand, the last peak observed at 490 °C is corresponding to the endothermic reaction which is mostly associated with removal of the residual nitrate used for the preparation of Ag_2O nanoparticles. Therefore, these obtained results indicated that the as-prepared Zeo@Ag_2O shows good thermal stability in the range of temperature between 25 and 250 °C.

The UV–Vis diffuse reflection spectroscopy technique is used to study the optical adsorption properties of Zeo@Ag_2O nanocomposite and the results are shown in Fig. 6a. Nevertheless, we could find that the as prepared Zeo@Ag_2O displayed an obviously a wide and strong light absorbance in the whole visible light region due to pure p-Ag_2O nanoparticles which is in good agreement with the previous reports [19, 43]. This attitude can give an excellent photocatalytic activity toward hazardous dyes. However, the band gap (Eg) of nanocomposite is calculated by fitting the corresponding absorption data using the following Kubelka–Munk equation:

$$(\alpha h\nu)^2 = A(h\nu - Eg)$$

where α is the absorption coefficient, A is constant, h is Planck constant, ν is light frequency, and Eg is the band gap energy.

Thus, the Eg of the Zeo@Ag_2O nanocomposite is estimated to be about 1.20 eV from the plot of $(\alpha h\nu)^2$ versus the photon energy ($h\nu$), as shown in Fig. 6b.

3.2 Photocatalytic Activity of as Prepared Zeo@Ag_2O

In order to investigate the photocatalytic degradation capability of Zeo@Ag_2O nanocomposite, the degradation of RhB in wastewater is examined under sunlight irradiation as a func-

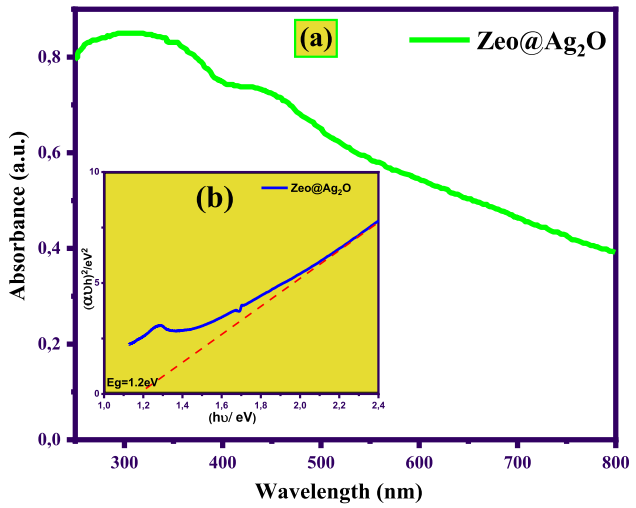

Fig. 6 **a** UV–vis–NIR diffuse reflectance spectra and **b** corresponding to plots of $(\alpha h\nu)^2$ versus the photon energy $(h\nu)$ of zeo@Ag_2O nanocomposite

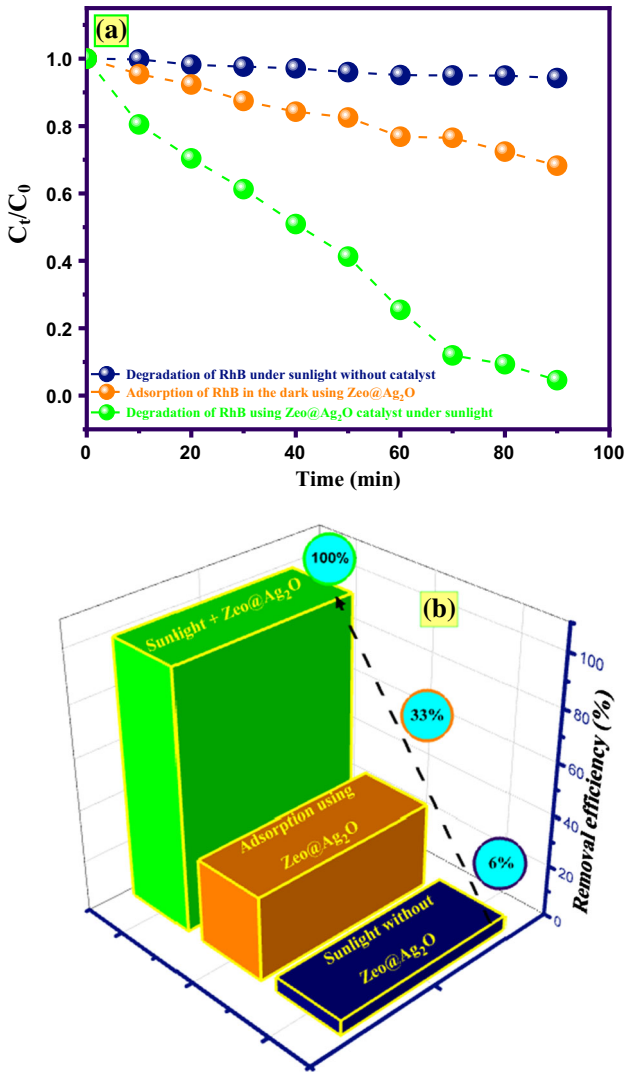

Fig. 7 **a** photolysis of RhB, adsorption of RhB using Zeo@Ag_2O in dark, and photocatalytic degradation of RhB using Zeo@Ag_2O under sunlight illumination curves; **b** the removal rate of RhB by photolysis, adsorption, and photocatalytic degradation process

tion of time. Figure 7a, b displays the Ct/C_0 versus time plots and the removal efficiency of RhB under sunlight without catalyst, Zeo@Ag_2O catalyst without sunlight (adsorption), and in the presence of Zeo@Ag_2O catalyst under sunlight, respectively. However, it can be seen that the photolysis efficiency (blank run) reveals a little reduction in the RhB concentration which is estimated to be approximately 6% under sunlight irradiation for 90 min. Thus, confirmed that direct photolysis has no effect on the removal of RhB dye from aqueous solution. Also, the adsorption capacity of the as-prepared nanocomposite is evaluated under the dark condition and it is found that only 33% of RhB dye can be eliminated within 90 min. This little adsorption capability of as-synthesized nanocomposite is partially referred to as the electrostatic interactions between cationic pollutant molecules and negative charge on zeolite surface. This negative charge of the surface is attributed to the existence of silanol and aluminol groups [44]. Afterward, the photocatalytic activity of Zeo@Ag_2O nanocomposite in the presence of solar light is investigated over the decomposition of hazardous RhB dye. It can be seen that the degradation efficiency increases rapidly and the results show about 100% of RhB dye is degraded in wastewater under 90 min of irradiation. Based on the obtained characterization results, the high photodegradation rate of hazardous RhB dye by Zeo@Ag_2O nanocomposite is contributed to the high dispersion of Ag_2O nanoparticles on the zeolite surface, which can reduce their agglomeration and then make these particles in more contact with RhB molecules. In this work, it is easy to conclude that the removal of RhB dye from wastewater can be improved by the synergy of adsorption and photocatalysis.

On the other hand, the photodegradation efficiency of our synthetized Zeo@Ag_2O nanocomposite is compared with other photocatalysts previously studied in the literature, Table 1. The activity of Ag_2O loaded Zeolite is high, as mentioned above, the presence of Ag_2O on the zeolite surface plays an important role in improving the degradation efficiency of RhB dye during 90 min of irradiation, which is high and fast compared to other photocatalysts.

3.3 Role of Reactive Oxygen Species and Possible Improved Photocatalytic Mechanism of Zeo@Ag_2O Nanocomposite

To study the photodegradation mechanism of hazardous RhB dye over Zeo@Ag_2O nanocomposite, the trapping experiments are firstly performed using different scavengers. Among them: EDTA-2Na (EDTA), L- acid ascorbic (ASC),

Table 1 Comparison of photocatalytic degradation of RhB dye using various photocatalysts

Photocatalyst	Light source	C_{RhB} (mg/L)	Degradation (%)	Time (min)	Ref
Ns-TiO_2 bilayer	UV–visible	4.8	50%	300	[45]
Fe_2O_3/H_2O_2	visible light	15	100%	180	[46]
g/ZnO /AgO/TiO_2 composite	UV–visible	10	99.3%	100	[47]
SnC5	Visible light	10	100%	125	[48]
Zeo@Ag_2O	Visible light	5	100%	90	This work

and Isopropanol alcohol (IPA) to quench hole (h^+), superoxide radicals ($^\circ O_2^-$), and hydroxyl radicals (HO°) in the photocatalytic reaction, respectively. As displayed in Fig. 8a, b, the degradation efficiency is significantly reduced from 100 to 13% and 39% after the addition of (4 mM) of EDTA and IPA into the system under sunlight irradiation, respectively. This indicated that both h^+ and HO° play a crucial role in the photodegradation process. Whereas, the removal of RhB is still up to ~ 85% with ASC as scavengers for superoxide radicals ($^\circ O_2^-$), which means that $^\circ O_2^-$ don't play an important role in photocatalytic degradation of RhB over Zeo@Ag_2O nanocomposite. Thus, the obtained results indicated that the order of photogenerated active species is h^+ > HO° > $^\circ O_2^-$.

On the other hand, the CB and VB edge potential of Ag_2O semiconductor photocatalyst are determined by using the Mulliken electronegativity theory to gain insight into the photocatalytic mechanism of Zeo@Ag_2O catalyst [22, 49].

$$\chi(A_aB_b) = \left[\chi(A)^a \cdot \chi(B)^b\right]^{\frac{1}{a+b}} \quad (2)$$

$$E_{CB} = \chi - E_0 - \frac{E_g}{2} \quad (3)$$

$$E_{VB} = E_{CB} - E_g \quad (4)$$

where χ (eV) is the absolute electronegativity of the semiconductor Ag_2O which is determined to be 5.29 eV, E_g is band gap energy of semiconductor and E_o is the free electrons of the energy on the standard hydrogen spectrum (~4.5 eV). E_{VB} (eV),EE_{CB} is the CB edge potential, E_{VB} is the VB edge potential of the semiconductor. According to the above equations, the E_{VB} and E_{CB} of Zeo@Ag_2O nanocomposite are determined to be 1.40 eV and 0.20 eV versus NHE, respectively.

Apparently, Zeo@Ag_2O nanocomposite with gap energy equal 1.20 eV can be excited by visible light irradiation. The photogenerated electrons in the conduction band could easily transfer to the valance band of as prepared nanocomposite and then the free electrons and holes could be generated in CB and VB, respectively. However, the negative surface of zeolite can play a crucial role to resolve the problem of recombination electron–hole pairs.

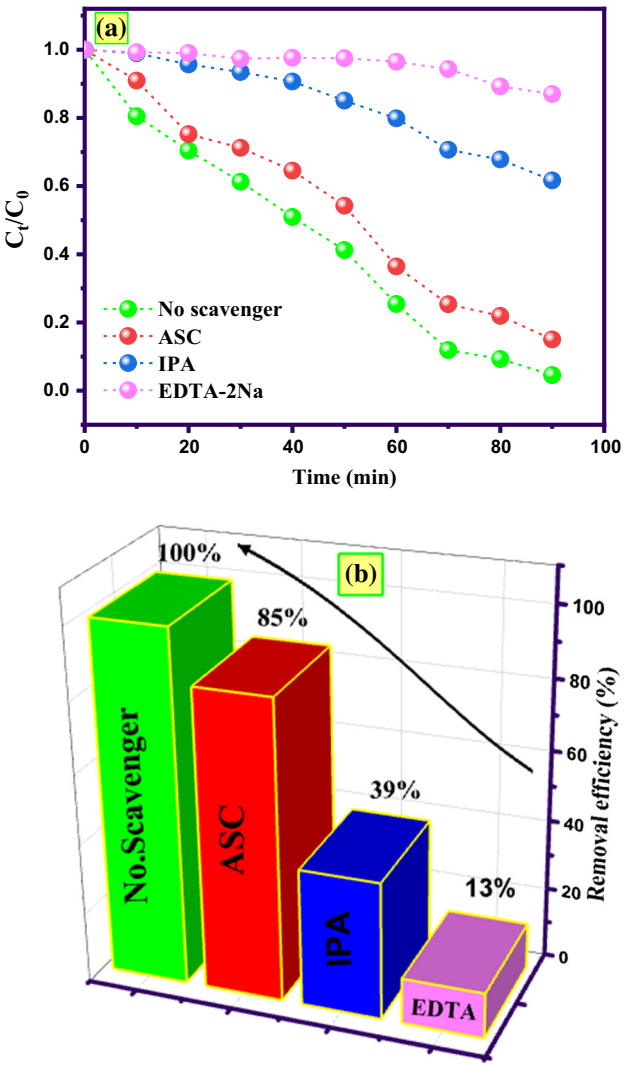

Fig. 8 The species trapping experiments for degradation of RhB over Zeo@Ag_2O nanocomposite

As can be seen in Fig. 9, the accumulated electrons in the CB of Zeo@Ag_2O nanocomposite with a potential 0.20 eV versus NHE could note reduce O_2 to produce $^\bullet O_2^-$ which is more positive than the standard redox potential of $O_2/^\bullet O_2^-$ (− 0.33 eV vs. NHE). While it can react with O_2 dissolved and produce H_2O_2 because of the more positive potential of O_2/H_2O_2 (+ 0.682 eV) and then H_2O_2 may react with

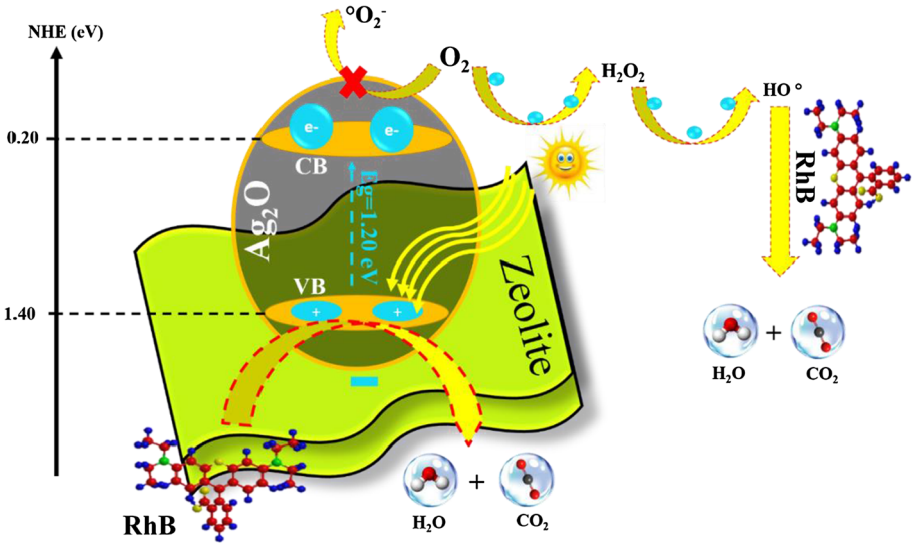

Fig. 9 The schematic drawing of the photocatalytic performance of Zeo@Ag2O nanocomposite

electrons to produce HO• radicals. However, because the CB potential of Zeo@Ag_2O is more negative than the potential of the OH/H_2O (~ 2.72 eV), the photogenerated holes cannot react with the OH• to produce OH^- but it can oxidize RhB molecules directly and produce simple molecules CO_2 and H_2O as explained in the following equations (Eq. 5–10).

$$\text{Zeo@Ag}_2\text{O} + h\nu \rightarrow \text{Zeo@Ag}_2\text{O}\,(e^-_{CB} + h^+_{VB}) \quad (5)$$

$$O_2 + e^-_{CB} \rightarrow {}^{\circ}O_2^- \quad (6)$$

$${}^{\circ}O_2^- + H_2O \rightarrow {}^{\circ}OOH + OH^- \quad (7)$$

$${}^{\circ}OOH + H_2O + e^-_{CB} \rightarrow H_2O_2 + OH^- \quad (8)$$

$$H_2O_2 + e^-_{CB} \rightarrow {}^{\circ}OH + OH^- \quad (9)$$

$$h^+ + \text{RhB dye} \rightarrow CO_2 + H_2O \quad (10)$$

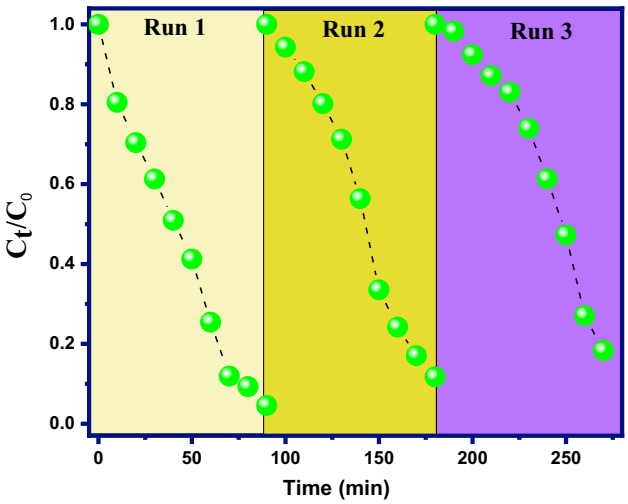

Fig. 10 Cycling runs for the photocatalytic degradation of RhB dye over Zeo@Ag_2O under visible-light irradiation

3.4 Evaluation of Stability

The stability and recyclability of any photocatalyst is a critical factor for their practical applications. Nevertheless, the photocatalytic degradation of RhB dye using Zeo@Ag_2O nanocomposite is investigated for 90 min at three time's cyclic experiments. In this work, the Zeo@Ag_2O nanocomposite used after each run is collected from aqueous media and washed several times with ethanol and water, and then dried in the electrical oven at 80 °C for the next use. As displayed in Fig. 10, it can be observed that Zeo@Ag_2O nanocomposite still has high photocatalytic activity toward hazardous Rhodamine B in aqueous media after three cycles, and the photocatalytic degradation efficiency of Zeo@Ag2O nanocomposite decreased from ≈ 100% in the first run to 88.3% and 81.7% in the 2nd run and 3rd run, respectively. This reveals that this nanocomposite has excellent stability under visible light illumination. The slight decrease in activity could be attributed to the loss of catalyst throughout the processes of recycling. Taken into account Ag_2O is used directly as a photocatalyst without support, it decomposed into weakly active Ag during O_2 evolution from water. In this work, the high stability can be due to the fact that the silver reduction was minimal during light irradiation which can be attributed to the negative surface of the zeolite. Therefore, the nanocomposite Zeo@Ag_2O photocatalyst can be considered as stable photocatalyst during the photocatalytic degradation process.

4 Conclusion

To summarize, the Zeo@Ag_2O nanocomposite is successfully prepared using a facile method and characterized using different techniques such as XRD, FTIR, SEM, EDX, BET, and UV–vis diffuse reflectance spectroscopy. Zeo@Ag_2O photocatalyst exhibited high photocatalytic efficiency for Rhodamine B dye degradation and achieved 100% in 90 min under visible light irradiation. Additionally, the Zeo@Ag_2O nanocomposite revealed high stability under sunlight irradiation after 3 runs. The obtained results demonstrated that the prepared photocatalyst can be considered eco-friendly and promising toward hazardous dyes in aqueous media.

Acknowledgements Authors are grateful to their institutions for providing facilities, support, and encouragement. This institutional collaboration is highly acknowledged.

Authors' contributions All authors contributed to the study's conception and design. Material preparation, data collection, and analysis were performed by F. Alakhras, E. Alhajri, T.A. Saleh, and H. Ouachtak. The original draft preparation was written by R. Haounati, A. Jada, and F. Alakhras, whereas review and editing of the manuscript were done by G. Al-Mazaideh, N. Hafid, and A.A. Addi. All authors read and approved the final manuscript.

Funding No funding has been received for this study.

Declarations

Conflict of interest The authors state that there is no conflict of interest regarding the publication of this paper.

References

1. Singh, A.; Kumar, S.; Panghal, V.; Arya, S.S.; Kumar, S. : Utilization of unwanted terrestrial weeds for removal of dyes. Rasayan J. Chem. **12**, 1956–1963 (2019). https://doi.org/10.31788/RJC.2019.1245401
2. Lellis, B.; Fávaro-Polonio, C.Z.; Pamphile, J.A.; Polonio, J.C.: Effects of textile dyes on health and the environment and bioremediation potential of living organisms. Biotechnol. Res. Innov. **3**, 275–290 (2019). https://doi.org/10.1016/j.biori.2019.09.001
3. Akhouairi, S.; Ouachtak, H.; Addi, A.A.; Jada, A.; Douch, J.: Natural sawdust as adsorbent for the eriochrome black T dye removal from aqueous solution. Water. Air. Soil Pollut. (2019). https://doi.org/10.1007/s11270-019-4234-6
4. Ouachtak, H.; Akhouairi, S.; Haounati, R.; Addi, A.A.; Jada, A.; Taha, M.L.; Douch, J.: 3,4-dihydroxybenzoic acid removal from water by goethite modified natural sand column fixed-bed: Experimental study and mathematical modeling. Desalin. Water Treat. **194**, 439–449 (2020). https://doi.org/10.5004/dwt.2020.25562
5. Largo, F.; Haounati, R.; Akhouairi, S.; Ouachtak, H.; El Haouti, R.; El Guerdaoui, A.; Hafid, N.; Santos, D.M.F.; Akbal, F.; Kuleyin, A.; Jada, A.; Addi, A.A.: Adsorptive removal of both cationic and anionic dyes by using sepiolite clay mineral as adsorbent: Experimental and molecular dynamic simulation studies. J. Mol. Liq. (2020). https://doi.org/10.1016/j.molliq.2020.114247
6. Samsami, S.; Mohamadi, M.; Sarrafzadeh, M.H.; Rene, E.R.; Firoozbahr, M.: Recent advances in the treatment of dye-containing wastewater from textile industries: overview and perspectives. Process Saf. Environ. Prot. **143**, 138–163 (2020). https://doi.org/10.1016/j.psep.2020.05.034
7. Bulgariu, L.; Escudero, L.B.; Bello, O.S.; Iqbal, M.; Nisar, J.; Adegoke, K.A.; Alakhras, F.; Kornaros, M.; Anastopoulos, I.: The utilization of leaf-based adsorbents for dyes removal: a review. J. Mol. Liq. **276**, 728–747 (2019). https://doi.org/10.1016/j.molliq.2018.12.001
8. Bharagava, R.N.; Chowdhary, P.: Emerging and eco-friendly approaches for waste management. Eco-Friendly Approaches Waste Manag, Emerg (2018) https://doi.org/10.1007/978-981-10-8669-4
9. Aljeboree, A.M.; Alshirifi, A.N.; Alkaim, A.F.: Kinetics and equilibrium study for the adsorption of textile dyes on coconut shell activated carbon. Arab. J. Chem. **10**, S3381–S3393 (2017). https://doi.org/10.1016/j.arabjc.2014.01.020
10. Assila, O.; Zouheir, M.; Tanji, K.; Haounati, R.; Zerrouq, F.; Kherbeche, A.: Copper nickel co-impregnation of Moroccan yellow clay as promising catalysts for the catalytic wet peroxide oxidation of caffeine. Heliyon. **7**, e06069 (2021)
11. Haounati, R.; Ouachtak, H.; El Haouti, R.; Akhouairi, S.; Largo, F.; Akbal, F.; Benlhachemi, A.; Jada, A.; Addi, A.A.: Elaboration and properties of a new SDS/CTAB@Montmorillonite organoclay composite as a superb adsorbent for the removal of malachite green from aqueous solutions. Sep. Purif. Technol. **255**, 117335 (2021). https://doi.org/10.1016/j.seppur.2020.117335
12. Al-Abbad E., Alakhras F. (2020) Removal of dye acid red 1 from aqueous solutions using chitosan-iso-vanillin sorbent material Indones. J. Sci. Technol.; 5: 352–365. https://doi.org/10.17509/ijost.v5i3.24986
13. El Haouti, R.; Ouachtak, H.; El Guerdaoui, A.; Amedlous, A.; Amaterz, E.; Haounati, R.; Addi, A.A.; Akbal, F.; El Alem, N.; Taha, M.L.: Cationic dyes adsorption by Na-Montmorillonite nano clay: experimental study combined with a theoretical investigation using DFT-based descriptors and molecular dynamics simulations. J. Mol. Liq. **290**, 111139 (2019). https://doi.org/10.1016/j.molliq.2019.111139
14. Kishor, R.; Purchase, D.; Saratale, G.D.; Saratale, R.G.; Ferreira, L.F.R.; Bilal, M.; Chandra, R.; Bharagava, R.N.: Ecotoxicological and health concerns of persistent coloring pollutants of textile industry wastewater and treatment approaches for environmental safety. J. Environ. Chem. Eng. **9**, 105012 (2021). https://doi.org/10.1016/j.jece.2020.105012
15. Gajanan, K.; Tijare, S.N.: Applications of nanomaterials. Mater. Today Proc. **5**, 1093–1096 (2018). https://doi.org/10.1016/j.matpr.2017.11.187
16. Saha, J.; Begum, A.; Mukherjee, A.; Kumar, S.: A novel green synthesis of silver nanoparticles and their catalytic action in reduction of Methylene Blue dye. Sustain. Environ. Res. **27**, 245–250 (2017). https://doi.org/10.1016/j.serj.2017.04.003
17. Xue, H.; Wang, K.; Bai, Y.; He, F.; Yang, H.; Wang, F.; Liu, P.: Preparation of novel Ag 2 O/Na 3 Bi(PO 4) 2 heterogeneous nanostructures with enhanced visible-light responsive photocatalytic activity. Mater. Lett. **242**, 39–41 (2019). https://doi.org/10.1016/j.matlet.2019.01.094
18. Gusain, R.; Gupta, K.; Joshi, P.; Khatri, O.P.: Adsorptive removal and photocatalytic degradation of organic pollutants using metal oxides and their composites: a comprehensive review. Adv. Colloid Interface Sci. **272**, 102009 (2019). https://doi.org/10.1016/j.cis.2019.102009
19. Li, Y.; Wang, Q.; Wang, H.; Tian, J.; Cui, H.: Novel Ag2O nanoparticles modified MoS2 nanoflowers for piezoelectric-assisted full solar spectrum photocatalysis. J. Colloid Interface Sci. **537**, 206–214 (2019). https://doi.org/10.1016/j.jcis.2018.11.013

20. Abdel-Khalek, A.A.; Mahmoud, S.A.; Zaki, A.H.: Visible light assisted photocatalytic degradation of crystal violet, bromophenol blue and eosin Y dyes using AgBr-ZnO nanocomposite. Environ. Nanotechnol. Monit. Manag. **9**, 164–173 (2018). https://doi.org/10.1016/j.enmm.2018.03.002
21. Ouachtak, H.; El Haouti, R.; El Guerdaoui, A.; Haounati, R.; Amaterz, E.; Addi, A.A.; Akbal, F.; Taha, M.L.: Experimental and molecular dynamics simulation study on the adsorption of Rhodamine B dye on magnetic montmorillonite composite γ-Fe2O3@Mt. J. Mol. Liq. **309**, 113142 (2020). https://doi.org/10.1016/j.molliq.2020.113142
22. Haounati, R.; El Guerdaoui, A.; Ouachtak, H.; El Haouti, R.; Boud-douch, A.; Hafid, N.; Bakiz, B.; Santos, D.M.F.; Labd Taha, M.; Jada, A.; Ait Addi, A.: Design of direct Z-scheme superb magnetic nanocomposite photocatalyst Fe3O4/Ag3PO4@Sep for hazardous dye degradation. Sep. Purif. Technol. **277**, 119399 (2021). https://doi.org/10.1016/j.seppur.2021.119399
23. Mani, M.; Harikrishnan, R.; Purushothaman, P.; Pavithra, S.; Rajkumar, P.; Kumaresan, S.; Al Farraj, D.A.; Elshikh, M.S.; Balasubramanian, B.; Kaviyarasu, K.: Systematic green synthesis of silver oxide nanoparticles for antimicrobial activity. Environ. Res. **202**, 111627 (2021). https://doi.org/10.1016/j.envres.2021.111627
24. Brabazon, D.; Pellicer, E.; Zivic, F.; Sort, J.; Baró, M.D.; Grujovic, N.; Choy, K.L.: Commercialization of nanotechnologies-A case study approach. (2017)
25. Dhand, V.; Soumya, L.; Bharadwaj, S.; Chakra, S.; Bhatt, D.; Sreedhar, B.: Green synthesis of silver nanoparticles using Coffea arabica seed extract and its antibacterial activity. Mater. Sci. Eng. C. **58**, 36–43 (2016). https://doi.org/10.1016/j.msec.2015.08.018
26. Wei, J.; Chen, Z.; Tong, Z.: Engineering Z-scheme silver oxide/bismuth tungstate heterostructure incorporated reduced graphene oxide with superior visible-light photocatalytic activity. J. Colloid Interface Sci. **596**, 22–33 (2021). https://doi.org/10.1016/j.jcis.2021.03.117
27. Shume, W.M.; Murthy, H.C.A.; Zereffa, E.A.: A review on synthesis and characterization of Ag2O nanoparticles for photocatalytic applications. J. Chem. (2020). https://doi.org/10.1155/2020/5039479
28. Jiang, W.; Wang, X.; Wu, Z.; Yue, X.; Yuan, S.; Lu, H.; Liang, B.: Silver oxide as superb and stable photocatalyst under visible and near-infrared light irradiation and its photocatalytic mechanism. Ind. Eng. Chem. Res. **54**, 832–841 (2015). https://doi.org/10.1021/ie503241k
29. Alakhras, F.; Alhajri, E.; Haounati, R.; Ouachtak, H.; Addi, A.A.; Saleh, T.A.: A comparative study of photocatalytic degradation of Rhodamine B using natural-based zeolite composites. Surf. Interfaces. **20**, 100611 (2020)
30. Petronella, F.; Truppi, A.; Ingrosso, C.; Placido, T.; Striccoli, M.; Curri, M.L.; Agostiano, A.; Comparelli, R.: Nanocomposite materials for photocatalytic degradation of pollutants. Catal. Today. **281**, 85–100 (2017). https://doi.org/10.1016/j.cattod.2016.05.048
31. Isari, A.A.; Payan, A.; Fattahi, M.; Jorfi, S.; Kakavandi, B.: Photocatalytic degradation of Rhodamine B and Real textile wastewater using Fe-doped TiO2 anchored on reduced graphene oxide (Fe-TiO2/rGO): characterization and feasibility, mechanism and pathway studies. Appl. Surf. Sci. (2018). https://doi.org/10.1016/j.apsusc.2018.08.133
32. Inglezakis, V.J.; Satayeva, A.; Yagofarova, A.; Tauanov, Z.; Meiramkulova, K.; Farrando-Pérez, J.; Bear, J.C.: Surface interactions and mechanisms study on the removal of iodide from water by use of natural Zeolite-based silver nanocomposites. Nanomaterials **10**, 1–23 (2020). https://doi.org/10.3390/nano10061156
33. Reeve, P.J.; Fallowfield, H.J.: Natural and surfactant modified zeolites: a review of their applications for water remediation with a focus on surfactant desorption and toxicity towards microorganisms. J. Environ. Manage. **205**, 253–261 (2018). https://doi.org/10.1016/j.jenvman.2017.09.077
34. Wang, Z.; Tan, K.; Cai, J.; Hou, S.; Wang, Y.; Jiang, P.; Liang, M.: Silica oxide encapsulated natural zeolite for high efficiency removal of low concentration heavy metals in water. Colloids Surfaces A Physicochem. Eng. Asp. **561**, 388–394 (2019). https://doi.org/10.1016/j.colsurfa.2018.10.065
35. Ruíz-Baltazar, A.; Esparza, R.; Gonzalez, M.; Rosas, G.; Pérez, R.: Preparation and characterization of natural zeolite modified with iron nanoparticles. J. Nanomaterials **2015**, 364763 (2015). https://doi.org/10.1155/2015/364763
36. Ouachtak, H.; El Guerdaoui, A.; Haounati, R.; Akhouairi, S.; El Haouti, R.; Hafid, N.; Ait Addi, A.; Šljukić, B.; Santos, D.M.F.; Taha, M.L.: Highly efficient and fast batch adsorption of orange G dye from polluted water using superb organo-montmorillonite: experimental study and molecular dynamics investigation. J. Mol. Liq. (2021). https://doi.org/10.1016/j.molliq.2021.116560
37. He, P.; Wang, W.; Du, L.; Dong, F.; Deng, Y.; Zhang, T.: Zeolite A functionalized with copper nanoparticles and graphene oxide for simultaneous electrochemical determination of dopamine and ascorbic acid. Anal. Chim. Acta. **739**, 25–30 (2012). https://doi.org/10.1016/j.aca.2012.06.004
38. Sing, K.S.W.: Reporting physisorption data for gas/solid systems with special reference to the determination of surface area and porosity. Pure Appl. Chem. **57**, 603–619 (1985). https://doi.org/10.1351/pac198557040603
39. Kuila, U.; Prasad, M.: Specific surface area and pore-size distribution in clays and shales. Geophys. Prospect. **61**, 341–362 (2013). https://doi.org/10.1111/1365-2478.12028
40. Raja, K.; Saravanakumar, A.; Vijayakumar, R.: Efficient synthesis of silver nanoparticles from Prosopis juliflora leaf extract and its antimicrobial activity using sewage. Spectrochim acta—part a mol. Biomol. Spectrosc. **97**, 490–494 (2012). https://doi.org/10.1016/j.saa.2012.06.038
41. Srirangam, G.M.; Parameswara Rao, K.: Synthesis and charcterization of silver nanoparticles from the leaf extract of *Malachra capitata* (L.). Rasayan J. Chem. **10**, 46–53 (2017). https://doi.org/10.7324/RJC.2017.1011548
42. Rosman, N.; Salleh, W.N.W.; Ismail, A.F.; Jaafar, J.; Harun, Z.; Aziz, F.; Mohamed, M.A.; Ohtani, B.; Takashima, M.: Photocatalytic degradation of phenol over visible light active ZnO/Ag2CO3/Ag2O nanocomposites heterojunction. J. Photochem. Photobiol. A Chem. **364**, 602–612 (2018). https://doi.org/10.1016/j.jphotochem.2018.06.029
43. Wen, X.J.; Niu, C.G.; Zhang, L.; Liang, C.; Zeng, G.M.: A novel Ag2O/CeO2 heterojunction photocatalysts for photocatalytic degradation of enrofloxacin: possible degradation pathways, mineralization activity and an in depth mechanism insight. Appl. Catal. B Environ. **221**, 701–714 (2018). https://doi.org/10.1016/j.apcatb.2017.09.060
44. Kuzniatsova, T.; Kim, Y.; Shqau, K.; Dutta, P.K.; Verweij, H.: Zeta potential measurements of zeolite Y: application in homogeneous deposition of particle coatings. Microporous Mesoporous Mater. **103**, 102–107 (2007). https://doi.org/10.1016/j.micromeso.2007.01.042
45. Zhuang, J.; Dai, W.; Tian, Q.; Li, Z.; Xie, L.; Wang, J.; Liu, P.; Shi, X.; Wang, D.: Photocatalytic degradation of RhB over TiO2 bilayer films: effect of defects and their location. Langmuir **26**, 9686–9694 (2010). https://doi.org/10.1021/la100302m
46. Kusior, A.; Michalec, K.; Jelen, P.; Radecka, M.: Shaped Fe 2 O 3 nanoparticles: synthesis and enhanced photocatalytic degradation towards RhB. Appl. Surf. Sci. **476**, 342–352 (2019). https://doi.org/10.1016/j.apsusc.2018.12.113
47. Bian, H.; Zhang, Z.; Xu, X.; Gao, Y.; Wang, T.: Photocatalytic activity of Ag/ZnO /AgO/TiO2 composite. Phys. E Low-Dimens. Syst. Nanostruct. (2020). https://doi.org/10.1016/j.physe.2020.114236

48. Ahmed, M.A.; Al-Zaqri, N.; Alsalme, A.; Glal, A.H.; Esa, M.: Rapid photocatalytic degradation of RhB dye and photocatalytic hydrogen production on novel curcumin/SnO2 nanocomposites through direct Z-scheme mechanism. J. Mater. Sci. Mater. Electron. **31**, 19188–19203 (2020). https://doi.org/10.1007/s10854-020-04455-8

49. Jourshabani, M.; Shariatinia, Z.; Badiei, A.: Synthesis and characterization of novel Sm 2 O 3 /S-doped g-C 3 N 4 nanocomposites with enhanced photocatalytic activities under visible light irradiation. Appl. Surf. Sci. **427**, 375–387 (2018). https://doi.org/10.1016/j.apsusc.2017.08.051